ISSN 1070-4272, Russian Journal of Applied Chemistry, 2018, Vol. 91, No. 1, pp. 150−158. © Pleiades Publishing, Ltd., 2018.

VARIOUS TECHNOLOGICAL PROCESSES

Hierarchically Structured Porous SnO_2/TiO_2 Materials with Design Controllable Phases and Enhanced Photocatalytic Activity[1]

Haoran Zhu[a], Heyi Shao[b], and Qingchun Zhao[c,*]

[a] *Hefei No. 9 High School, 230601 Anhui, PR China*
[b] *Hefei No. 45 Middle School, 230001 Anhui, PR China*
[c] *School of Materials and Chemical Engineering, Anhui Jianzhu University Hefei 230022 Anhui, PR China*
** e-mail: qczhao@ahjzu.edu.cn*

Received January 16, 2017

Abstract—To increase the photogenerated carrier separation and reduce the electron-hole recombination process for photocatalysts performance. In this article, hierarchically macroporous structured TiO_2/SnO_2 materials with controllable composition and phases have been successfully synthesized by using a typical process. This method involves several sequential preparation steps: (1) preparation of core-shell structure SnO_2/PS submicrospheres by hydrothermal method; (2) preparation of TiO_2/SnO_2/PS submicrospheres by assembling amorphous TiO_2 on surface of SnO_2/PS submicrospheres; (3) direct calcination of TiO_2/SnO_2/PS submicrospheres to eventually produce hierarchically structured TiO_2/SnO_2 materials with pores-in-pores. With rutile phases TiO_2, TiO_2/SnO_2 macroporous materials show significantly enhanced catalytic activity when used as photocatalysts for the degradation of Rhodamine B under UV irradiation. The photodegradation ratio of Rhodamine B was 96% for 25 min.

DOI: 10.1134/S1070427218010238

INTRODUCTION

During the past decade, lots of novel hybrid materials with hierarchical porosity and structures have attracted considerable attention because of their potential applications in photocatalysis [1–3], supercapacitor [4], energy conversion [5–9], H_2 production, and sensors [10, 11]. Among the various porous structures, hierarchical macroporous structured materials due to their unique structure with pores-in-pores exhibit some unique physical and chemical properties. For example, by the fine hierarchization of the nanostructure and chemical composition at different scales, reactivity and light harvesting can be enhanced since it has been found that in macro and mesoporous TiO_2 materials the acrochannels acted as a light-transfer path for introducing incident photon flux onto the inner surface of mesoporous TiO_2. This allowed light waves to penetrate deep inside the photocatalysts making it a more efficient light harvester. In addition, the high porosity, large pore volume, and the interconnected pore structure of macroporous hierarchical materials can facilitate the interfacial- and transport-related process for the fast mass transport, efficient electrolyte permeation, and fast electron transport [12–16].

TiO_2 is one of the most widely studied semiconducting oxide materials for a wide range of applications including bioseparation [17], sensing[18], hydrogen production[19], solar energy conversion [20], lithium storage [21–23], photocatalysis and catalysis [24, 25]. Since the discovery of its catalytic activity for hydrogen production from water [26], TiO_2 has also been intensively studied and widely used for water splitting and environmental treatment [27–30]. However, because of the poor electron transport characteristics of TiO_2 (0.1–1 $cm^2 V^{-1} s^{-1}$), TiO_2 photocatalyst has an inherent and significant drawback, which consists in the fact that the photogenerated charge carriers [electron (e^-)–hole (h^+) pairs] can recombine. Therefore, to increase the photocatalytic activity of TiO_2 it is important to decrease the recombination of photogenerated charge carriers. By

[1] The text was submitted by the authors in English.

comparison, SnO_2 has been extensively studied due to higher electron mobility (100–500 $cm^2 V^{-1} S^{-1}$) and a larger band gap (3.6 eV), which create fewer oxidative holes in the valence band [31]. However, the application of SnO_2 as photocatalyst has been limited due to poor performance: a faster interfacial electron recombination and lower trapping density, on the other hand, SnO_2 has a lower isoelectric point.

To increase the photogenerated carrier separation and reduce the electron-hole recombination process for photocatalysts performance, in this work controllable phases of SnO_2/TiO_2 hierarchically structured porous materials were realized by growth control during the synthesis procedure. In this research, two main reasons contributed to the outstanding photocatalysts performance. First, the acrochannels of macro and mesoporous TiO_2/SnO_2 materials acted as a light-transfer path for introducing incident photon flux onto the inner surface of mesoporous TiO_2. This allowed light waves to penetrate deep inside the photocatalyst making it a more efficient light harvester. Second, the electron transfer efficiency was improved by the involvement of high conductive SnO_2 nanoparticles, and the direct and effective electron delivery from TiO_2 to SnO_2 nanoparticles further.

EXPERIMENTAL

Synthesis of monodisperse copolymer submicrospheres. Monodisperse copolymer submicrospheres were prepared via emulsifier-free emulsion polymerization method. Using 0.148 g $(NH_4)_2S_2O_8$ as initiator, 7.7 g styrene, 1.5 g vinyl benzyl chloride, 0.5 g divinylbenzene and 0.0389 g sodium *p*-styrenesulfonate as monomers, 200 g water and 0.1388 g $NaHCO_3$, were mixed in a flask with a magnetic stirring. The mixture was bubbled with N_2 for 40 min to eliminate oxygen before it was sealed. The mixture was heated at 76°C for 24 h. The system was then allowed to cool to room temperature. The final products were collected and washed with water and alcohol to remove any possible ionic remnants, and then dried at 60°C for 24 h. Experimental results indicate that well-defined copolymer submicrospheres can be obtained.

Synthesis of polyvinyl benzyl mercaptan submicrospheres (PS). Ethanol (17 g) solution containing 7.3 g sulfourea was added to 20 g toluene containing 4 g copolymer submicrospheres [32]. The mixture was heated at 50°C for 20 h in a flask with a magnetic stirring. The obtained products were washed with 20% NaOH aqueous solution and methanol three times, respectively. The polyvinyl benzyl mercaptan submicrospheres (PS) were obtained.

Synthesis of core-shell structure SnO_2/PS submicrospheres. $SnCl_2$ (0.1 g), H_2O_2 (0.1 g), 0.1 g urea, and 0.1 g polyvinyl benzyl mercaptan submicrospheres were immersed in deionized water (25 g) with a magnetic stirring for 30 min. The mixture was transferred into a 50 mL teflon-lined autoclave. The autoclave was sealed and maintained at 180°C for 24 h. After the reaction, the autoclave was naturally cooled to room temperature and the precipitates were collected and washed several times with distilled water and absolute ethanol. The final products were dried under vacuum at 60°C for 8 h. After these processes, core-shell structure SnO_2/PS submicrospheres were prepared by covering a layer of SnO_2 on the surface of the polyvinyl benzyl mercaptan submicrospheres.

Synthesis of TiO_2/SnO_2/PS submicrospheres and hierarchically structured SnO_2/TiO_2 porous materials

TiO_2/SnO_2/PS submicrospheres were prepared by assembling amorphous TiO_2 on surface of SnO_2/PS submicrospheres. In a typical synthesis, 2.0 g core-shell structure SnO_2/PS submicrospheres were immersed in 20 g ethanol solution containing different amounts of tetra-*n*-butyl titanate (1.5, 2.0, 2.5, and 3.0 g) and magnetically stirred for 24 h. The solution was dried in air. The obtained samples (nos. 1–4) were heated to 550°C at a rate of 5°C/min in air then held for 3 h and cooled to room temperature.

Photocatalytic activity tests. The photocatalytic degradation of Rhodamine B (Rh B) was carried out to evaluated the photocatalytic activity of the obtained hierarchically structured TiO_2/SnO_2 porous materials. Before the photocatalytic reaction was initiated, the hierarchically structured TiO_2/SnO_2 porous materials were irradiated with UV light for 30 min to remove any residual organic compounds. The aqueous system containing Rh B (2.0×10^{-5} M, 50 mL) and photocatalyst (20 mg) was magnetically stirred in the dark for 30 min to reach the adsorption equilibrium of Rh B on the surface of photocatalyst and then exposed to UV light from a 15 W UV lamp (254 nm) as the UV light source for different time. After centrifugation, 5 mL residual solution was taken out. The concentrations of Rh B solution were determined on a UV-Vis-8000S spectrophotometer.

Material characterization. A scanning electron microscope (SEM, Hitachi JSM-6700F) coupled with

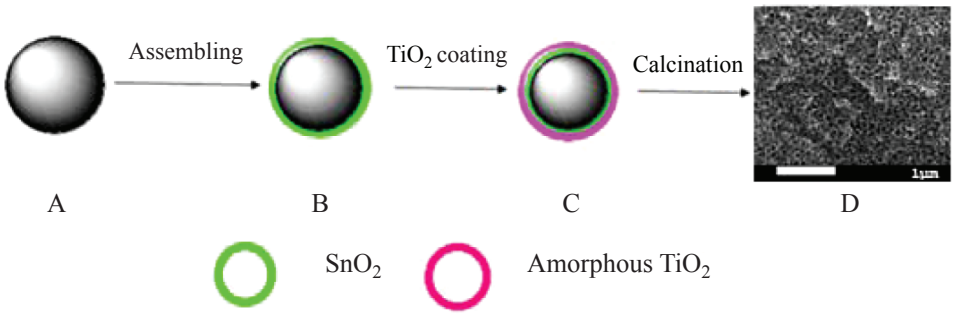

Fig. 1. Schematic illustration showing the general strategy for the synthesis of hierarchically structured TiO_2/SnO_2 porous materials. (A) Copolymer submicrosphere; (B) core-shell structure SnO_2/PS submicrosphere prepared by hydrothermal method; (C) TiO_2/SnO_2/PS submicrosphere prepared by assembling amorphous TiO_2 on surface of SnO_2/PS submicrosphere; (D) SEM image of obtained hierarchically structured TiO_2/SnO_2 porous materials.

energy-dispersive X-ray spectroscopy (EDX) was used to study the morphologies and composition of SnO_2/PS and TiO_2/SnO_2/PS submicrospheres. A high resolution TEM (JEOL 2011, operating at 200 kV) was used to analyze the microstructure of hierarchically structured SnO_2/ TiO_2 porous materials. In addition, the phase composition of the obtained products was studied by X-ray diffraction (XRD) using a Siemens D5000 diffractometer with CuK_α radiation (λ = 1.54178 Å).

RESULTS AND DISCUSSION

Hierarchically structured TiO_2/SnO_2 porous materials in this study were synthesized by two steps: self-assembly and calcination procedure, as shown in Fig. 1. In general this method involves: (1) core-shell structure SnO_2/PS submicrospheres were prepared by hydrothermal method; (2) core-shell structure SnO_2/PS submicrospheres were coated by amorphous TiO_2 layer to form TiO_2/SnO_2/PS submicrospheres; (3) directl calcination of TiO_2/SnO_2/PS submicrospheres to finally produce hierarchically structured TiO_2/SnO_2 porous materials.

The field emission scanning electron microscopy (FE-SEM) images were taken on a JEOL JSM-6700F SEM. Figure 2 is a typical SEM image of the obtained copolymer submicrospheres which clearly shows that copolymer composite is of sphere structure. SEM observation shows that copolymer submicrospheres with an average diameter of 200 nm. The standard deviation of the size distribution is less than 5%. The SEM (Fig. 2a) micrograph reveals that optimization of the experimental parameters is observed. Figure 3 shows XRD pattern of obtained core-shell structure SnO_2/PS submicrospheres.

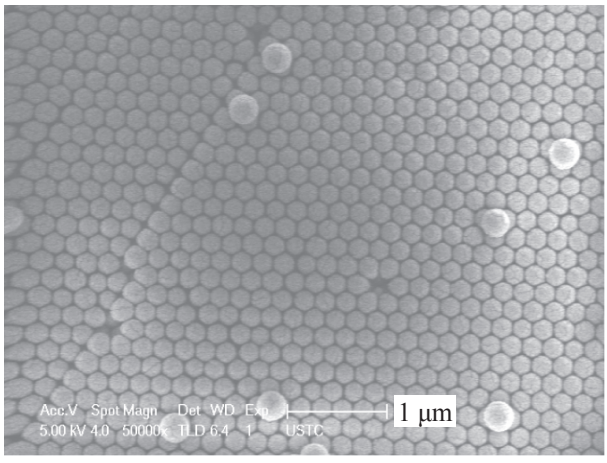

Fig. 2. SEM image of obtained copolymer submicrospheres allowing macroscopic preparation of monodisperse copolymer submicrospheres.

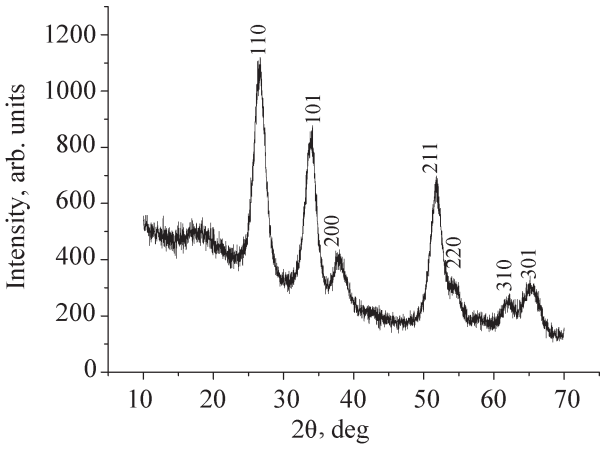

Fig. 3. XRD pattern of obtained core-shell structure SnO_2 / PS submicrospheres.

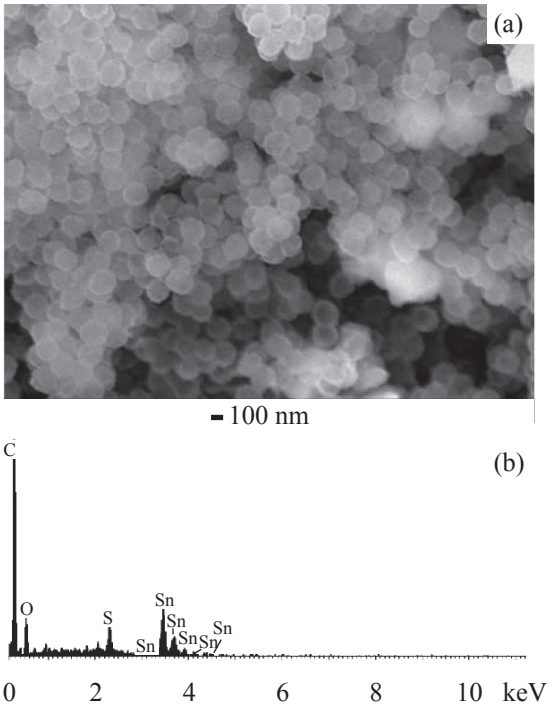

Fig. 4. (a) SEM image of obtained copolymer submicrospheres covered with a layer of SnO_2; (b) EDX analysis of the as-obtained submicrospheres covered with a layer of SnO_2.

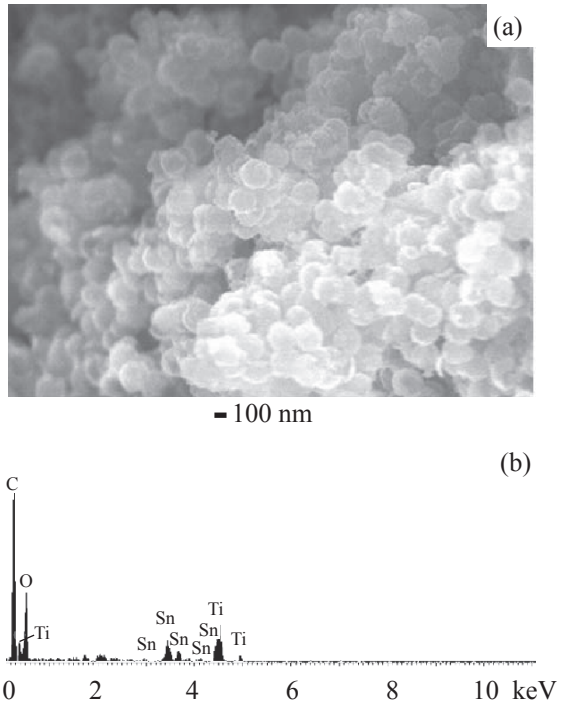

Fig. 5. (a) SEM image of obtained TiO_2/SnO_2/PS submicrospheres with yolk–shell structure (no. 1); (b) EDX analysis of the as-obtained TiO_2/SnO_2/PS submicrospheres.

Peaks at 2θ = 26.96, 34.01, 38.13, 51.82, 54.24, 62.00, and 65.31°, which are attributed, respectively, to the (110), (101), (200), (211), (220), (310), and (301) planes of crystalline structure of tetragonal SnO_2. All the diffraction peaks of SnO_2/PS submicrospheres can be very well indexed to a rutile structure of SnO_2 [space group: *P*42/mnm (136), JCPDS No. 41-1445].

Figure 4a shows a scanning electron microscopy (SEM) image of core-shell structure SnO_2/PS submicrospheres. From the SEM image according to the XRD result we can see that the surface of the submicrospheres was covered by SnO_2 and turned into not smooth. We suppose the most likely mechanism for synthesis of SnO_2. In the presence of H_2O, O_2, and urea, Sn^{2+} ions are oxidated and hydrolyzed. The reactions sequentially occur as follows:

$$2Sn^{2+} + O_2 + 4OH^- \rightarrow 2SnO_2 + 2H_2O$$

The obtained SnO_2 nanoparticles were synthesized on the surface of polyvinyl benzyl mercaptan submicrospheres by assembling. Core-shell structure SnO_2/PS submicrospheres were obtained. The composition of the submicrospheres covered by a layer of SnO_2 was identified by energy-dispersive X-ray spectroscopy (EDX) measurement (Fig. 4b). The EDX spectrum shows there was no Cl, indicating $SnCl_2$ were completely hydrolyzed.

From SEM image of submicrospheres TiO_2/SnO_2/PS (Fig. 5a) we can see the surface of the submicrospheres TiO_2/SnO_2/PS turns into not smooth. The colloidal titanium dioxide was obtained by tetra-*n*-butyl titanate reaction with water in air. The composition of the TiO_2/SnO_2/PS was identified by energy-dispersive X-ray spectroscopy (EDX) measurement (Fig. 5b). Quantitative analysis of the EDX spectrum gives that the colloidal titanium dioxide was obtained.

Figure 6a is a typical SEM image of hierarchically structured TiO_2/SnO_2 porous materials synthesized by calcination of TiO_2/SnO_2/PS (no. 1) submicrospheres at 550°C in air. It clearly shows that obtained products possess alveolate structure. The magnified SEM image (Fig. 6) revealed that the diameters of the macropores were in a range of 90–130 nm and were remarkably small compared with original copolymer submicrospheres of diameter approximately ca. 200 nm. That is due to

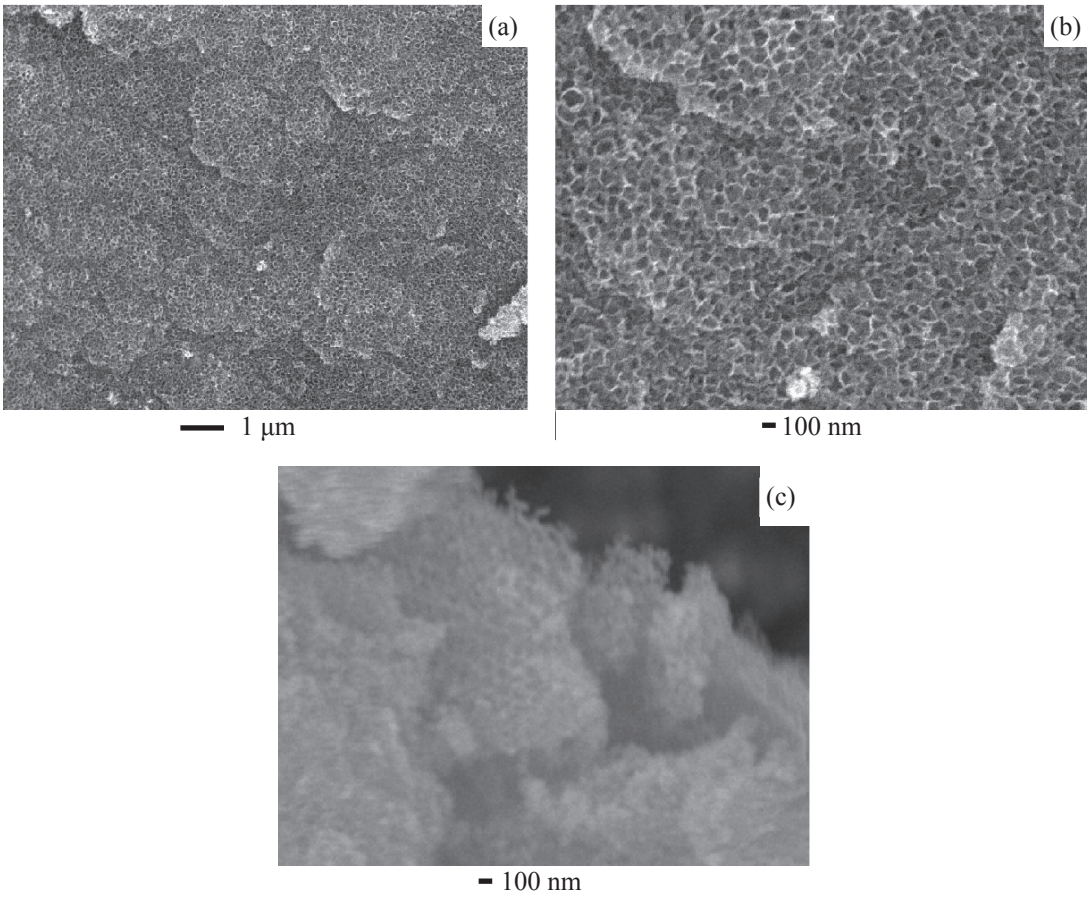

Fig. 6. SEM images of obtained hierarchically structured TiO_2/SnO_2 porous materials. Surface of obtained hierarchically structured TiO_2/SnO_2 porous materials: (a) SEM image; (b) magnified SEM image; (c) SEM image of the fracture surface.

the shrinkage of the TiO_2/SnO_2 network during the calcination process. The thickness of hole wall is about 20–25 nm. Form the SEM image of the fracture surface of hierarchically structured TiO_2/SnO_2 porous materials (Fig. 6c) we can see the inside of the obtained materials is of pores-in-pores structure.

Figures 7a–7c show the SEM images of hierarchically structured TiO_2/SnO_2 macroporous materials obtained from calcination (nos. 2–4) at 550°C in air. All of the obtained products are of alveolate structure and the thickness of the hole wall rises with increasing the TiO_2 content.

The crystalline phases and sizes of the hierarchically structured TiO_2/SnO_2 porous materials can be evaluated from X-ray diffraction (XRD) spectra. From Fig. 8a we can see the XRD pattern of hierarchically structured TiO_2/SnO_2 porous materials with obvious peaks at 2θ = 26.96, 34.01, 38.13, 39.15, 52.01, and 63.68° which are attributed, respectively, to the (110), (101), (200), (111), (211), and (112) planes of crystalline structure of tetragonal SnO_2.

Characteristic XRD peaks of rutile TiO_2 appeared at 2θ = 27.30, 35.86, 41.18, 54.14, and 68.93°, which are attributed to the (110), (101), (111), (211), and (301) planes of crystalline structure, respectively. Those results will confirm the fact of hierarchical structuring of porous materials with TiO_2 and SnO_2 nanocrystallites. Based on Scherer's formula we can calculate the average sizes of the nanoparticles consisting of obtained porous materials from the full-width at half-maximum (FWHM) of characteristic XRD peaks. Derived from the FWHM of 34.01 at the (101) peak of SnO_2 and 35.76 at the (210) peak of TiO_2, nano-SnO_2 and TiO_2 particles in hierarchically structured TiO_2/SnO_2 porous materials were calculated to have a mean size of 8.16 and 6.45 nm, respectively. This result is in agreement with that observed from the transmission electron microscopy (TEM) images.

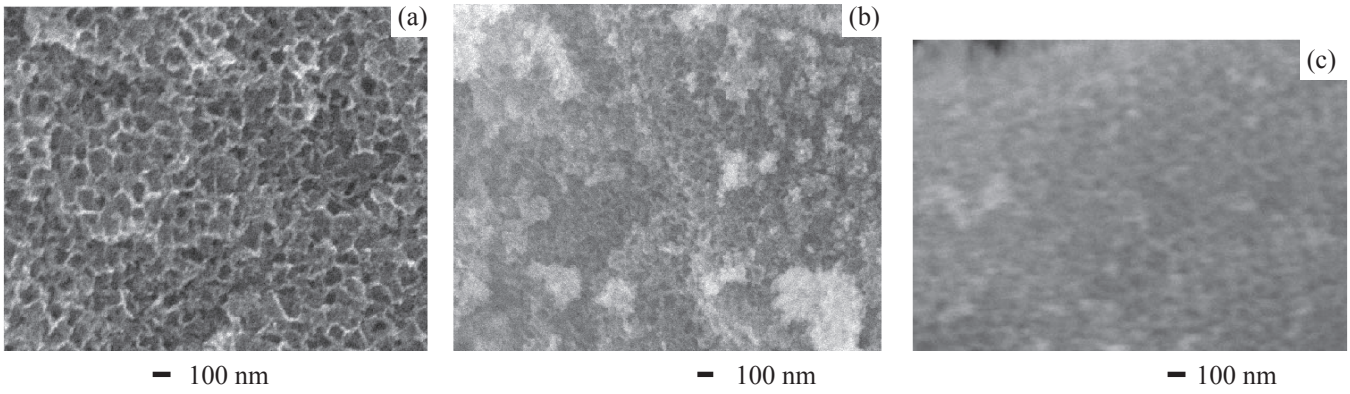

Fig. 7. (a–c) SEM images of hierarchically structured TiO_2/SnO_2 macroporous materials obtained from calcination nos. 2–4 at 550°C in air.

Figures 8b–8d are the X-ray diffraction spectra of the SnO_2/TiO_2 porous materials obtained by calcination (nos. 2–4) at 550°C in air. The XRD patterns of SnO_2/TiO_2 porous materials show obvious peaks at 2θ = 26.96, 34.01, 38.13, 39.15, 52.01, and 63.68° which are attributed to the (110), (101), (200), (111), (211) and (112) planes of crystalline structure of tetragonal SnO_2, respectivel, and the peaks at 2θ = 25.30, 37.90, 48.03, 53.97, 55.13, and

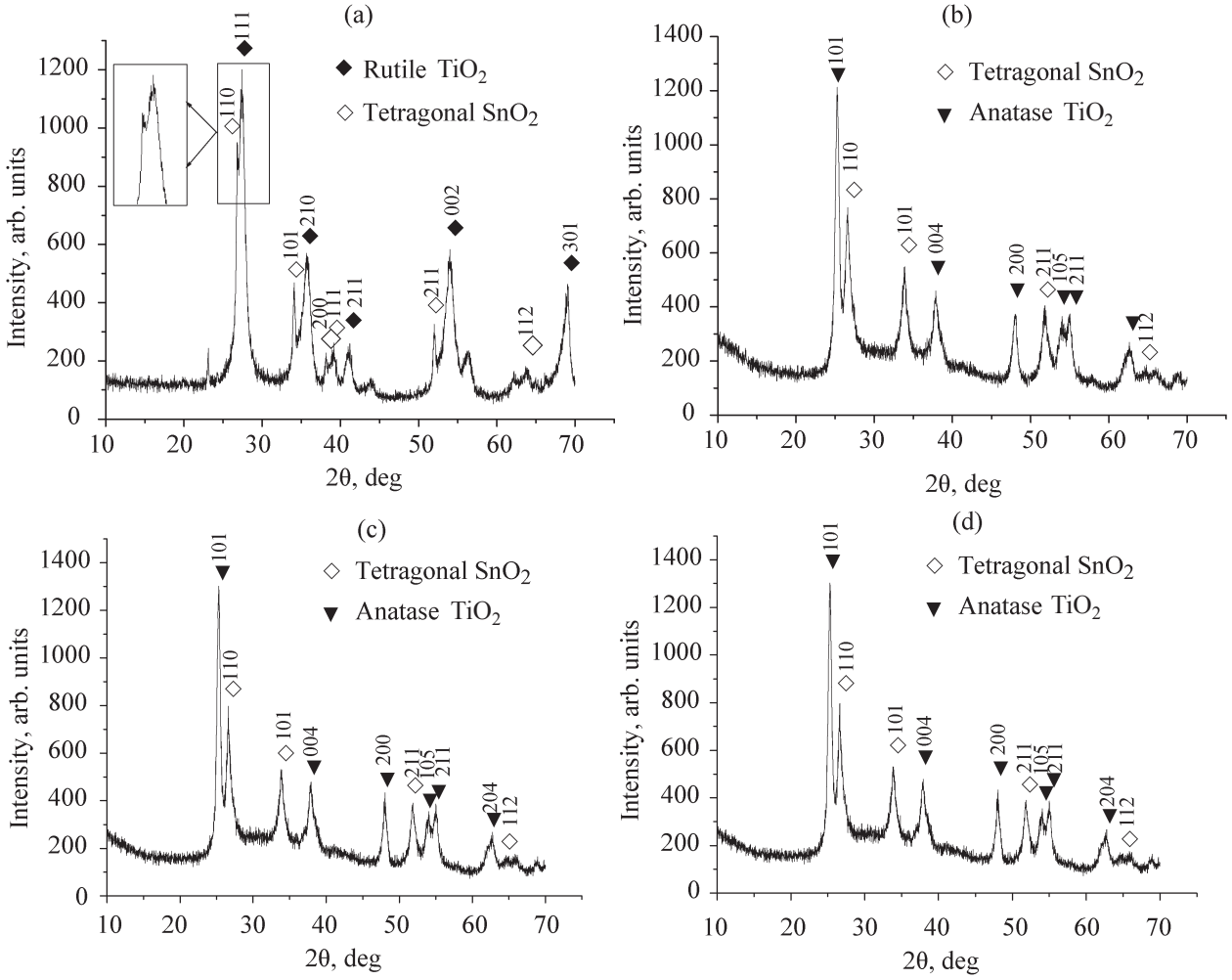

Fig. 8. (a–d) XRD pattern of obtained hierarchically structured TiO_2/SnO_2 porous materials obtained from calcination nos. 1–4 at 550°C in air.

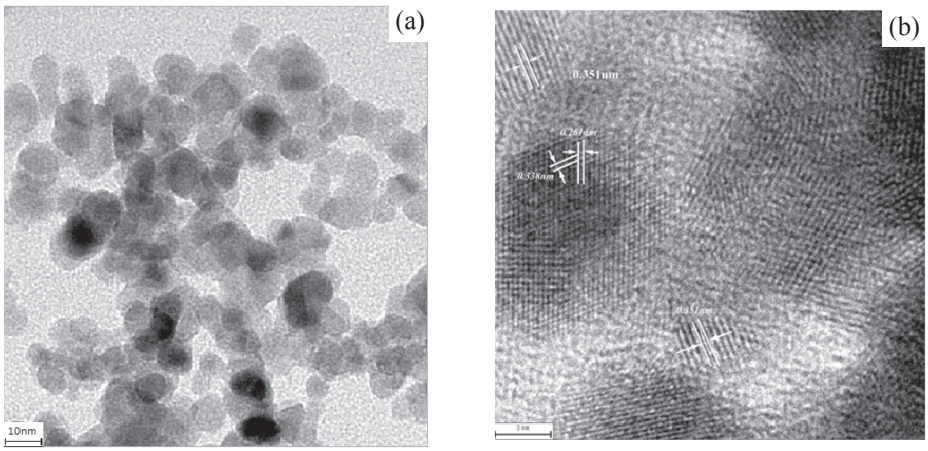

Fig. 9. (a) HRTEM image of obtained hierarchically structured TiO_2/SnO_2 porous materials obtained from calcination no. 1 at 550°C in air. (b) HRTEM image of the lattice fringes.

62.71 which are attributed to the (101), (004), (200), (105), (211) and (112) planes of crystalline structure of anatase TiO_2. It is worth noting (Figs. 8b–8d), there were not other peaks indicating that the pure phase TiO_2/SnO_2 porous materials can be obtained. Derived from the FWHM of 34.01 at the (101) peak of SnO_2 and 25.35 at the (101) peak of TiO_2, nano-SnO_2 particles in hierarchically structured TiO_2/SnO_2 porous materials were calculated to have a mean size of 8.16 nm. TiO_2 nanoparticles have a mean size of 9.72, 11.50, and 13.01 nm, respectively. It means that sizes of TiO_2 nanoparticles increase with TiO_2 content increase.

For further detailed structural analysis of TiO_2/SnO_2 porous materials, high-resolution transmission electron microscopy (HRTEM) images were obtained and analyzed (Figs. 9a and 9b). From HRTEM image of TiO_2/SnO_2 porous materials obtained from calcination yolk–shell structure TiO_2/SnO_2/PS submicrospheres (no.1) at 550°C in air (Fig. 9a) we can see that irregularly shaped nanoparticles with diameters of 5–10 nm were observed. The nanoparticles were connected to each other and formed pores-in-pores structure.

As shown in Fig. 9b the *d*-spacings of the lattice fringes were found to be about 0.339 and 0.263nm, corresponding to the (110) and (101) planes of tetragonal rutile phase SnO_2, respectively. These values are also close to the (110) and (101) planes of rutile TiO_2 with interplanar spacings of 0.325 and 0.249 nm, respectively. Therefore, Those results will further testify that the porous materials are constructed from TiO_2 and SnO_2 nanoparticles.

To investigate the effect of SnO_2 nanoparticles on photocatalytic activity of TiO_2/SnO_2 porous materials catalysts for Rh B degradation, the performance of all the TiO_2/SnO_2 porous materials catalysts and the TiO_2 samples (nos. 11, 22, 33, and 44) obtained from removal of SnO_2 from the calcined nos. 1–4 for Rh B degradation were compared.

The performance of the photocatalysts toward Rh B degradation, measured by monitoring the adsorption intensity of the 554 nm peak vs. different intervals irradiation time, is shown in Fig. 10a. The catalysts obtained from calcination nos. 1–4 at 550°C in air have a different adsorption capacity in the range of 5–9% of C/C_0. Hierarchically structured TiO_2/SnO_2 porous materials catalyst obtained from calcination no. 1 at 550°C in air has a biggest adsorption capacity for Rh B. Degradation was significantly decreased when TiO_2/SnO_2 porous materials catalysts with TiO_2 content increase were employed in the reaction system. As shown in Fig. 10a, the relative photocatalytic activity of the catalysts for Rh B degradation follows the order: no. 1 > no. 2 > no. 3 > no. 4: no. 1 > no. 11, no. 2 > no. 22, no. 3 > no. 33, no. 4 > no. 44. By combining XRD data (Fig. 8), one can notice that the performance enhancement is mainly due to the decrease in TiO_2 content and formation of a TiO_2/SnO_2 mixed composite. The charge separation of electrons and holes is without doubt the most important factor in determining the photophysical properties of TiO_2. The values of E_g (E_g is the bandgap in the bulk) for the rutile and anatase forms are 3.0 and 3.2 eV, respectively [33]. Although rutile TiO_2 can absorb a broader range of light due to the smaller band gap than anatase, electron-

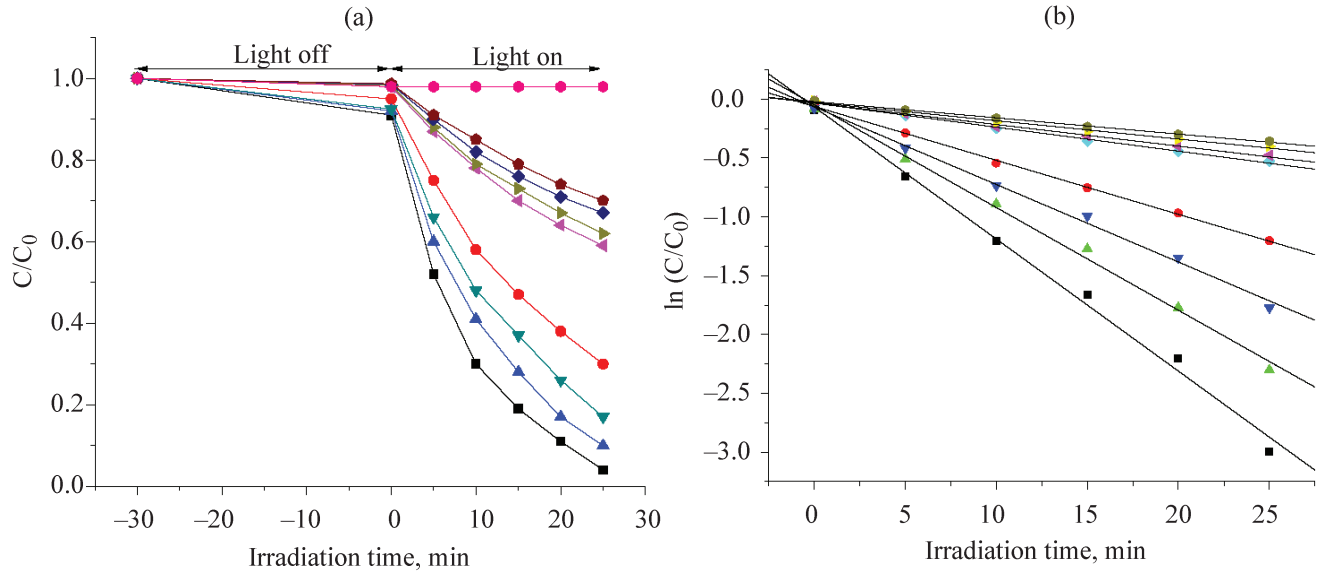

Fig. 10. (a) Evolution of Rh B concentration and (b) apparent reaction rate constant vs. UV irradiation time in the presence of different ierarchically structured TiO_2/SnO_2 porous materials catalysts and SnO_2 obtained from calcination (■) no. 1, (▲) no. 2, (▼) no. 3, (●) no. 4 and core-shell structure SnO_2/PS submicrospheres (⬟) at 550°C in air, respectively. TiO_2 [(◀) no. 11, (▶) no. 22, (◆) no. 33, (⬟) no. 44] were obtained by removal of SnO_2 from the calcined nos.1–4 at 550°C in air (TiO_2/SnO_2 porous materials was dispersed in an aqueous hydrochloric acid solution (20 mL, 2 M), which was then stirred for 4 h at 25°C. The etched TiO_2/SnO_2 porous materials were centrifuged and washed several times with deionized water and ethanol and dried under vacuum to obtain the final powder).

hole pairs initiated by light absorption in the rutile TiO_2 are easier recombination than in anatase [34, 35], The photophysical properties of anatase TiO_2 is better than the rutile. Our obtained catalysts own hierarchically structured TiO_2/SnO_2 porous materials. The electron transport characteristics of TiO_2 (0.1–1 $cm^2\ V^{-1}\ s^{-1}$) is poorer than those of SnO_2 (100–500 $cm^2\ V^{-1}\ s^{-1}$), TiO_2 surfaces combinations with SnO_2 semiconductor are beneficial in decreasing the electron and hole recombination rate and thereby increasing the quantum yield of the photocatalytic process [30].

In order to compare the reaction kinetics, the ln (C/C_0) vs. reaction time t for different hierarchically structured TiO_2/SnO_2 porous materials catalysts was shown in Fig.10b. The linear correlation coefficient values R^2 obtained by linear regression are 0.9935, 0.9953, 0.9953, 0.9990, 0.9952, 0.9942, 0.9556, 0.9969. All these plots match the first-order reaction kinetics, the reaction rate constants k can be calculated from the rate equation $\ln (C/C_0) = -kt$, and the k values were 0.11214, 0.08721, 0.06586, 0.04579, 0.02038, 0.01829, 0.01551, and 0.01378, respectively. The constant k continuously decreased as TiO_2 content increased. Hierarchically structured TiO_2/SnO_2 porous materials obtained from calcination no. 1 at 550°C in air showed the largest k value, indicating the highest photocatalytic efficiency.

CONCLUSIONS

Hierarchically macroporous structured TiO_2/SnO_2 materials with controllable composition and phases were successfully synthesized and further their performance was investigated in photocatalysis. The method involved producing the core-shell structure SnO_2/PS submicrospheres by hydrothermal method, followed by assembling for preparation yolk–shell structure TiO_2/SnO_2/PS submicrospheres, and, finally, calcination of yolk–shell structure TiO_2/SnO_2/PS submicrospheres to prepare the hierarchically structured TiO_2/SnO_2 porous materials. The as-prepared hierarchically structured TiO_2/SnO_2 porous materials show significantly enhanced photocatalytic activity in the degradation of Rh B molecules with rutile phase TiO_2.

REFERENCES

1. Zhao, J., Zou, Y., Zou, X., Ba,i T., Liu, Y., Gao, R., Wang, D., and Li, G-D., *Nanoscale*, 2014, vol. 6, pp. 7255–7262.
2. Chen, J.S., Chen, C., Liu, J., Xu, R., Qiao, S. Z., and Lou, X.W., *Chem. Commun*., 2011, vol. 47, pp. 2631–2633.
3. Yue, D.T., Qian, X.F., and Zhao, Y.X., *Science Bulletin,* 2015, vol. 60. no. 21, pp. 1791–1806.

4. Ding, S., Zhu, T., Chen, J. S., Wang, Z., Yuan, C., and Lou, X.W., *J. Mater. Chem*., 2011, vol. 21, pp. 6602–6606.
5. Sung, H.A., Dong, J.K., Won, S.C., and Jong, H.K., *Adv. Mater.,* 2013, vol. 25, pp. 4893–4897.
6. Umang, V.D., Xu, C., Wu, J., and Gao, D., *J. Phys. Chem.* C, 2013, vol. 117, pp. 3232–3239.
7. Karuturi, S.K., Luo, J., Cheng, C., Liu, L., Su, L.T., Tok, A.I.Y., and Fan, H.J., *Adv. Mater.,* 2012,vol. 24, pp. 4157–4162.
8. Pang, A., Sun, X., Ruan, H., Li, Y., Dai, S., and Wei, M., *Nano Energy*, 2014, vol. 5, pp. 82–90.
9. Wu, W., Xu, Y., Rao, H.S., Feng, H., Su, C., and Kuang, D., *Angew. Chem*., 2014, vol. 126, pp. 4916–4921.
10. Liu, B., Liu, L., Lang, X., Wang, H., Lou, X.W., and Eray, S.-A., *Energy Environ. Sci.,* 2014, vol. 7, pp. 2592–2597.
11. Lee, S., Lee, J., Hwang, S.-H., Yun, J., and Jang, J., *ACS Nano*, 2015, vol. 9, no. 5, pp. 4939–4949.
12. Chen, H.Y., Kuang, D.B., and Su, C.Y., *J. Mater. Chem*. 2012, vol. 22, pp. 15475–15489.
13. Zhang, Q.F. and Cao, G.Z., *Nano Today*, 2011, vol. 6, pp. 91–109.
14. O'Regan, B. and Gratzel, M., *Nature*, 1991, vol. 353, pp. 737–740.
15. Wang, Y.F., Li, K.N., Xu, Y.F., Rao, H.S., Su, C.Y., and Kuang, D.B., *Nanoscale*, 2013, vol. 5, pp. 5940–5948.
16. Qian, J., Liu, P., Xiao, Y., Jiang, Y., Cao, Y., Ai, X., and Yang, H., *Adv. Mater*., 2009, vol. 21, pp. 3663– 3667.
17. Lu, Z., Ye, M., Li, N., Zhong, W., and Yin, Y., *Angew. Chem., Int. Ed*., 2010, vol. 49, pp. 1862–1866.
18. Lu, Z., Duan, J., He, L., Hu, Y., and Yin, Y., *Anal. Chem*., 2010, vol. 82, pp. 7249–7258.
19. Nozik, A.J., *Nature*, 1975, vol. 257, pp. 383–386.
20. Satyanarayana, R-G., Krishnamoorthy, A., Christopher, Y., Michael, G., and Palani, B., *Energy Environ. Sci*., 2010, vol. 3, pp. 838–845.
21. Kuppan, S., Krishnamoorthy, A., and Palani, B., *Energy Environ. Sci.,* 2010, vol.3, pp. 939–948.
22. Kim, G., Jo, C., Kim, W., Chun, J., Yoon, S., Lee, J., and Choi, W., *Energy Env. Sci*., 2013, vol. 6, pp. 2932–2938.
23. Zhang, G., Wu, H-B., Song, T., Paik, U., and Lou, X., *Angew. Chem., Int. Ed.* 2014, vol. 53, no. 46, pp. 12590–12593.
24. Tripathy, J., Lee, K., and Schmuki, P., *Angew. Chem., Int. Ed*., 2014, vol. 53, no. 46, pp. 12605–12608.
25. Maximilian, M., Izabela, C., Núria, L., and Javier, P., *Angew. Chem., Int. Ed*., 2014, vol. 53, no. 33, pp. 8628–8633.
26. Fujishima, A. and Honda, K., *Nature*, 1972, vol. 238, pp. 37–38.
27. Zuo, F., Wang, L., Wu, T., Zhang, Z., Borchardt, D., and Feng, P., *J. Am. Chem. Soc*., 2010, vol. 132, pp. 11856–11857.
28. Zhou, W., Li, W., Wang, J., Qu, Y., Yang, Y., Xie, Y., Zhang, K., Wang, L., Fu, H., and Zhao, D., *J. Am. Chem. Soc*., 2014, vol. 136, no. 26, pp. 9280–9283.
29. Joo, J.B., Zhang, Q., Dahl, M., Lee, I., Goebl, J., Zaera, F., and Yin, Y., *Energy Environ. Sci*., 2012, vol. 5, pp. 6321–6327.
30. Liu, H., Joo, J.B., Dahl, M., Fu, L., Zeng, Z., and Yin, Y., *Energy Environ. Sci*., 2015, vol. 8, pp. 286–296.
31. Tiwana, P., Docampo, P., Johnston, M.B., Snaith, H.J., and Herz, L.M., *ACS Nano*, 2011, vol. 5, pp. 5158–5166.
32. Zhao, Q.C., *Appl. Sur. Sci.,* 2015, vol. 344, pp. 107–111.
33. Shen, Q., Katayama, K., Sawada, T., Yamaguchi, M., Kumagai, Y., and Toyoda, T., *Chem. Phys. Lett.,* 2006, vol. 419, pp. 464–468.
34. Jenny, S., Masaya, M., Masato, T., Zhang, J., Yu, H., Masakazu, A., and Detlef, W.B., *Chem. Rev*., 2014, vol. 114, pp. 9919–9986.
35. Amy, L. L., Lu, G., and John, T.Y., *Chem. Rev*., 1995, vol. 95, pp. 735–758.